も検出不可となる．

残念ながら，我が国の GWAS への対応は遅れていると言っていいだろう．1,000 例を超す症例で GWAS を行った報告はない．また，個々の研究者が有する症例数は，GWAS に耐えうる数ではないようである．日本でも多施設共同研究の推進が急がれるし，アジア全体を見据えた共同研究を行う研究体制も考慮していかなければならない．

わずかな効果の間違いない感受性遺伝子の検出

膨大な検体数での GWAS は，わずかな差ながら確実な遺伝要因の検出を統計的頑健さで可能とした．表1を再び参照いただきたい．有意差の強い SNP が示されているが，オッズ比は 1.2 ～ 1.6 と小さいことが見て取れるだろう．では，そのわずかな違いは意味があるのだろうか，また個人差医療へ利用できるのであろうか．遺伝要因は生まれながら有する危険因子かつ原因そのものなので，関与する遺伝子から病気のメカニズムをうかがい知ることができる．通常，*in vitro*, *in vivo* での機能的解析により，感受性遺伝子多型がどのように疾患にかかわるかの検討が行われる．オッズ比 1.2 ～ 1.6 くらいの多型では生物学的実験で 10 ～ 20 % 程度の差にしかならず，その検出は現実的に困難である．中年以降の発症なら，発症まで長年遺伝要因の影響を受けてきたことは想像できるだろう．いわゆる蓄積があるので，一時的な実験で示すことは困難となる．しかしながら，原因遺伝子同定により疾患に関与するパスウェイを知ることができ，当然治療ターゲットになる可能性がある．また，環境要因との相互作用解析から，関与する環境要因をあぶりだし，予防に役立てることが期待できる．

また，病巣となっている組織でマイクロアレイ解析による網羅的遺伝子発現が検討されている．遺伝的要因となっている遺伝子発現は病巣において変化していることが予想され，ゲノム全域における SNP 解析と遺伝子発現を組み合わせた検討がなされるであろう．

集団の階層化

アソシエーション・スタディでは集団階層化が問題となる．患者と対照の遺伝背景を同一にすることにより，患者＝疾患との関連をとら

えることができる．よく言われる例え話がある．サンフランシスコベイエリアにおいて，箸の使い方のうまさとヒト白血球抗原（HLA）との関連を調べた．結果，HLA－A1 タイプと箸をうまく使える形質が関連していた．HLA－A1 は chopstick gene だった？ もちろんそんなことはなく，サンフランシスコでのスタディ集団は中国系と白人集団が混在しており，中国系集団では HLA－A1 頻度が高いことによりこのような結論となった．言うまでもなく，集団中に混在していた中国系集団が箸をうまく使う．このような極端な例はないだろうが，わずかな差を検出するアソシエーション・スタディにおいて集団の階層化は常に大きな問題で注意を要する．日本人集団は均一性の高い集団と考える向きもある．比較の問題ではあるが，予想していたよりは多様性が高いと思った方がよい．そのためには対象とする集団の階層化を事前に確認しなければいけない．少ない数の遺伝子多型をタイピングしていた時代には検出できなかったことであるが，30 万～50 万 SNP をタイピングする時代となり，わずかな集団の階層化を精度良く確認できるようになった．

Purcell, et al の提唱している方法での検討例を示そう．ゲノム全域のほぼ独立な（連鎖不平衡にない）SNP セットを用いて個体対の同状態（identical by state：IBS）アリルの共有数をカウントし，IBS 共有割合を個体間の類似性の尺度として用いるものである．IBS 0 は {AA, aa} の対，IBS 1 は {Aa, AA} または {Aa, aa} の対，IBS 2 は {Aa, Aa}, {AA, AA} または {aa, aa} の対のように数える．これを 1 から引いたものを個体間の IBS 距離とする．IBS 距離をすべての標本対に対して計算することにより，IBS 距離行列が得られる．これはサンプルサイズを N とすると，N×N 対称行列である．この IBS 距離行列は，サンプル内のすべての個体間の相対距離を表しており，個体間の関係性を最大で N－一次元空間で表現していることになる．IBS 距離行列の持つ多次元情報を，より情報量が多く，個体間の関係性（特に離れ具合に着目する）を有効に表現できる低次元射影を可視化する 1 つの方法として，多次元尺度法（multidimensional scaling）がある．これは統計解析パッケージ R（http://www.r-project.org）などを用いれば簡単に実行できる．多次元尺度法を日本人標本と韓国人

図2 日本人標本と韓国人標本からなるデータに対する多次元尺度法の適用例

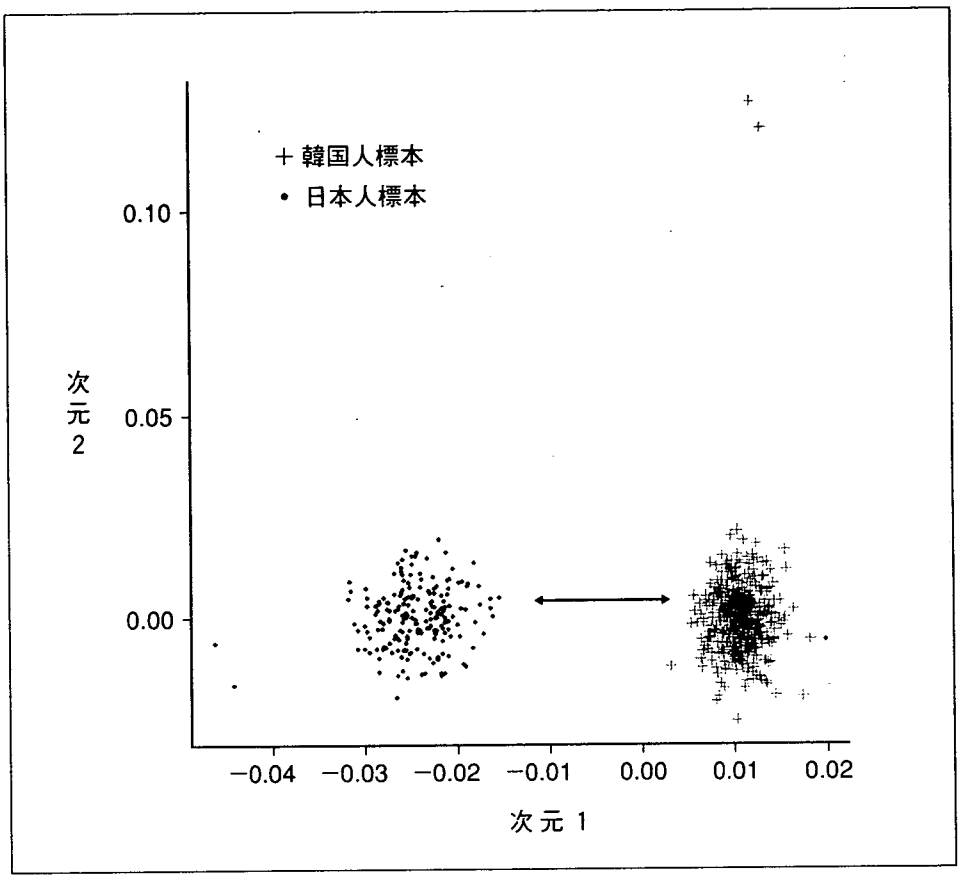

欧米人やアフリカ人などと比べると相対的に非常に小さなスケールでの違いであるが，くっきりと分離している．この程度の違いでもアリル頻度分布は劇的に異なる．プロット上部の韓国人標本の2個体は，類似性が比較的高く，ほぼ第2親等程度の血縁関係が示唆される．そのため，その個体対の距離が主クラスターに属する個体との距離に比べて相対的に小さすぎてしまい，はずれた点に位置する結果となったと考えられる．なお，縦軸と横軸のスケールの違いにも注意されたい．

標本からなるサンプルに適用した例を図2に示す．日本人と韓国人では集団に大きな違いがあることが見て取れるだろう．

おわりに

ここまで述べたことの繰り返しになるが，多因子疾患の遺伝解析は今，時代の大きなうねりの中にある．ゲノム全域アソシエーション・スタディにより，わずかな差であるが確実な遺伝子多型を検出できるようになり，新たな治療法の開発，予防法の開発が加速されることは疑いない．疾患遺伝子研究は収穫期を迎えている．今は刈り込みに集中する時期かもしれないが，得られた成果をどのように利用するか，

特に遺伝子間相互作用の検出など開発すべき問題が山積みである.

文　献

1) Risch N, et al: The future of genetic studies of complex human diseases. Science 273: 1516–1517, 1996.
2) The Wellcome Trust Case Control Consortium: Genome-wide association study of 14,000 cases of seven common diseases and 3,000 shared controls. Nature 447: 661–678, 2007.
3) Lander E S: The new genomics: global views of biology. Science 274: 536–539, 1996.
4) Cohen J C, et al: Multiple rare alleles contribute to low plasma levels of HDL cholesterol. Science 305: 869–872, 2004.

J Neurosurg Spine 7:184–193, 2007

Thoracic ossification of the human ligamentum flavum: histopathological and immunohistochemical findings around the ossified lesion

TAKAFUMI YAYAMA, M.D., D.M.SC.,[1] KENZO UCHIDA, M.D., D.M.SC.,[1] SHIGERU KOBAYASHI, M.D., D.M.SC.,[1] YASUO KOKUBO, M.D., D.M.SC.,[1] RYUICHIRO SATO, M.D.,[1] HIDEAKI NAKAJIMA, M.D., D.M.SC.,[1] TAKAHARU TAKAMURA, M.D.,[1] ALEXANDER BANGIRANA, M.D., M.MED.,[2] HIROSHI ITOH, M.D., D.M.SC.,[3] AND HISATOSHI BABA, M.D., D.M.SC.[1]

Departments of [1]Orthopaedics and Rehabilitation Medicine and [3]Pathological Sciences, Fukui University Faculty of Medical Sciences, Fukui, Japan; and [2]Department of Orthopaedic Surgery, Makerere University School of Medicine, Kampala, Republic of Uganda

Object. The object of this study was to histopathologically and immunohistochemically characterize ossification of the ligamentum flavum (OLF) in samples of the thoracic spine harvested en bloc during surgery and to enhance the understanding of the ossifying process, particularly calcification and ossification.

Methods. Samples of OLF plaque were obtained en bloc from 43 patients who underwent posterior decompression. The histopathological findings were correlated with radiological subtypes using computed tomography. The expression of type I and type II collagens, vascular endothelial growth factor (VEGF), transforming growth factor (TGF)β, and bone morphogenetic protein (BMP)–2 was investigated.

Results. Surgical decompression using the posterior floating and en bloc resection technique resulted in neurological improvement in 40 of 43 patients. Progression of the OLF lesion longitudinally and medially was associated with significant degeneration of elastic fibers, fiber bundle derangement, decrements in fiber diameter, and fragmentation. Calcification and ossification paralleled the degeneration of the elastic fibers, extended more medially, and fused in the central area. Expression of BMP-2, TGFβ, and VEGF was significant in chondrocytes in the calcified cartilage and fibrocartilage layers, especially around the calcified front.

Conclusions. Histopathologically, the progress of calcification and ossification was closely associated with the degeneration of elastic fibers and with significant expression of BMP-2, TGFβ, and VEGF in the ossification front. *(DOI: 10.3171/SPI-07/08/184)*

KEY WORDS • calcification • histopathology • immunohistochemistry • ligamentum flavum • ossification • thoracic spine

OSSIFICATION of the ligamentum flavum of the human spine progresses insidiously over a long period of time and can eventually cause devastating and serious compromises to the spinal cord.[1,2,6,9,16,27,32,35] Ossification of the ligamentum flavum was first described by Polgär[21] as early as 1920, and several investigators have since described the possible contribution of mechanical,[12,30] metabolic,[4,11,28] and cell biological factors[10,13,19,36] to the development and progression of OLF. A number of studies have also focused on the role of genetic factors in the pathogenesis of OLF,[22,26] based on the selectively high prevalence of the condition in certain geographic areas and racial groups.[1,3,14,17,23] Thus, there is an increased interest in understanding the underlying mechanisms of ossifying plaques in OLF and OPLL, including possible genetic associations as well as a search for candidate genes. Recently, linkage and linkage disequilibrium analyses[22,26] identified 35 candidate genes (such as collagen *COL6A1* and *COL11A2* genes) in patients with cervical OPLL, presumably including OLF. The exact mechanism of ligament ossification, however, remains poorly understood although the importance of genetic and biological factors has been acknowledged.

Abbreviations used in this paper: BMP = bone morphogenetic protein; CT = computed tomography; JOA = Japanese Orthopaedic Association; MR = magnetic resonance; OLF = ossification of the ligamentum flavum; OPLL = ossification of the posterior longitudinal ligament; PBS = phosphate-buffered saline; TGF = transforming growth factor; VEGF = vascular endothelial growth factor.

Histopathologically, proliferation of small blood vessels (neovascularization) and clustering of abnormal fibrocartilage and cartilaginous cells, with considerable metachromasia as well as hypertrophy of elastic fibers, were reported to reflect significant changes heralding the development of OLF.[4,8,12,37] Investigators have speculated that, in the presence of currently unknown factors, mesenchymal fibroblasts or fibroblast-like cells of the ligamentum flavum proliferate in an as yet unqualified abnormal manner. Recently investigators[12,30] found that spinal ligament cells, despite not carrying genetic information, could change their cytological sensitivities under repetitive distraction stress and then transform their osteogenetic properties of gene expression, resulting in initiation and development of OLF. The mechanisms that induce such cellular proliferation are not clear, but may involve specific osteogenetic cytokines and mechanical stimuli as well as certain metabolic disorders. These metaplastic cells in the ligament may eventually transform into osteoblasts, which contribute to the early development of OLF.

The present study was designed to investigate the histopathological features of human OLF specimens harvested en bloc during surgery. Specifically, we examined the immunohistological properties of the OLF plaque, ossification and calcification fronts, and the ligamentous enthesis to adjacent vertebral laminae.

Materials and Methods

Patient Population

Between 1991 and 2006, 43 patients were admitted to our University Medical Center for surgical treatment of OLF-related thoracic myelopathy. These patients included 20 men and 23 women with an average age at surgery of 61.8 years (range 38–77 years). None of the patients had evidence of congenital bone or joint disorders or musculoligamentous tissue abnormalities. None of the patients had a positive rheumatoid factor test or hyperparathyroidism. Twelve patients (28%) had diabetes mellitus (fasting blood sugar level $\geq$ 150 mg/dl). None of the patients was undergoing treatment with bisphosphonate, glucocorticoids, or etidronate sodium. A systemic radiographic survey confirmed the absence of ankylosing spondylitis or other seronegative spondyloarthropathies, calcium pyrophosphate crystal deposition,[38,39] diffuse idiopathic skeletal hyperostosis, or Paget disease.

Neurological assessment was conducted by two independent observers (H.N., K.U.), using the American Spinal Injury Association motor grading system modified from the Frankel classification, and a modified JOA scoring system[33] (Table 1). In the JOA scoring system, Category I (pain score of 3 points) was excluded because OLF rarely correlates with back pain. Thus, the highest possible score was 14 points. Neurological follow-up ranged from 6 months to 13 years (average 3.8 years). The demographic data of the patients are listed in Table 2.

Radiological examination methods included plain radiography, tomography, CT, and high-resolution MR imaging (1.5-tesla Signa, General Electric); occasionally myelography was performed using water-soluble contrast. Based on the CT classification of thoracic OLF described previously,[18,23] the lesions were classified as lateral, extended, enlarged, fused, or tuberous types (Fig. 1a–e). One-level OLF involvement was encountered in 20 patients; two levels were involved in 14, and three levels or more in nine patients. Seven patients had thoracic OLF combined with OPLL. The exact level or levels responsible for the myelopathy was determined using MR imaging or myelograms and epidural spinal cord evoked potentials, particularly in multilevel involvement. Occlusion of the subarachnoid space, flattening of the spinal cord, and the presence of high signal intensity within the spinal cord were assessed during myelopathy localization on MR images. The presence of abnormalities in two negative spikes (N1 and N2) in the epidural spinal cord evoked potentials was used to determine the level or levels of myelopathy.[5]

TABLE 1

Author's modification of the JOA scoring system for assessment of myelopathy

Categories	Score (point)
I. vertebral pain	
incapacitating and uncontrollable	0
controllable with medication	1
painful but no need of medication	2
absent	3
II. motor function of the lower extremity	
unable to walk	0
needs a cane or other walking aid on flat ground	1
needs walking aid only on stairs	2
able to walk unaided, but slowly	3
normal	4
III. sensory function	
(a) trunk	
apparent sensory disturbance	0
minimal sensory disturbance	1
normal	2
(b) lower extremity	
apparent sensory disturbance	0
minimal sensory disturbance	1
normal	2
IV. bladder function	
urinary retention or incontinence	0
severe dysuria (sense of retention)	1
slight dysuria (pollakiuria, retardation)	2
normal	3

* The score in a normal subject is the total of the best scores in each category, as follows: (I + II + III + IV) = 14 points.

Surgical Procedure and OLF Sample Harvesting

A sample of OLF was obtained using a posterior midline approach followed by exposure of the vertebral laminae and interlaminar levels. The spinous processes and posterior cortices of the laminae neighboring the OLF lesion were resected using a high-speed diamond bur. The inner cortices of the laminae near the OLF lesion were then cut or resected using a high-speed surgical airtome or a micro-Kerrison rongeur with a blade length of 2 mm and a thickness of 1 mm (Eagle). The OLF lesion often extended laterally, just medial to the facet joint, and thus approximately one third of the spinal canal side of the facet joint at the affected level was then resected, followed by incision of the inner cortex of the far lateral side of the lamina. The OLF lesion was then isolated and floated posteriorly on the dura like an "island."[5] At that stage, an epidural electrode pair (Unique Medical) was introduced for spinal cord monitoring at sites approximately 4 to 6 cm proximally and distally away from the OLF lesion. Fine-tipped skin hooks were then applied to the sides of the OLF lesion to carefully lift the ossified plaque dorsally away from the dura (Fig. 2 *left*) before it was finally resected (Fig. 2 *right*). When the dura was also ossified it was sometimes resected, preserving the arachnoid membrane. In four cases with OLF and OPLL, circumspinal decompression[29] was performed (Cases 5, 7, 28, and 40; Table 2).

All surgeries were performed by one of two senior spine surgeons (41 cases by H.B. and two cases by S.K.) using essentially the same technique. The first author (T.Y.) was responsible for all histopathological and immunohistochemical processing, and the findings were further evaluated by two independent board-certified special-

TABLE 2

*Summary of demographic data in 43 patients with thoracic OLF**

Case No.	Age (yrs), Sex	JOA Score (preop/ at FU)	Frankel–ASIA Grade (preop/ at FU)	Type of Paresis	Other Ossification	Levels of OLF	Type of OLF	Levels Decompressed	Surgical Remarks	Surgical Complication	FU (yrs)
1	49, F	7/10	D/E	spastic, para	OPLL C4–7	T11–12	fused	T11–12			5.7
2	59, F	6/7	C/C	spastic, para		T7–12	fused	T7–12			4.5
3	67, F	5/9	B/D	spastic, para		T10–12	extended	T10–12			4.5
4	58, F	7/0	C/A	flaccid, para		T8–L1	tuberous	T8–L1	blood loss 1350 g, dura mater ossification	transient SCI	3.9
5	38, F	5/6	C/C	spastic, B-S	OPLL T1–7	T2–12	fused	T1–8	circumspinal decompression		3.5
6	50, F	5/8	C/D	flaccid, epiconus	OPLL T1–6	T10–L1	lateral	T10–L1			7.0
7	62, M	8/10	D/E	spastic, para	OPLL T2–4	T4–5	enlarged	T1–6	circumspinal decompression		13.0
8	73, F	8/11	D/E	spastic, epiconus		T9–11	fused	T11–12	pedicular screwing		7.0
9	57, F	6/10	C/D	spastic, para		T8–L1	tuberous	T9–L1	dura mater ossification		3.3
10	69, M	6/10	D/E	spastic, para		T4–6, T8–11	lateral	T8–12			3.8
11	49, M	7/10	C/E	flaccid, mono	OPLL T8–10	T4–6	fused	T4–5	superficial wound infection		4.1
12	53, M	6/8	C/D	spastic, para		T10–12	enlarged	T10–12			3.5
13	62, F	7/8	D/D	spastic, para		T10–12	fused	T10–11			6.8
14	50, F	5/7	C/D	spastic, para	OPLL C4–1	T3–5	tuberous	T2–6			8.2
15	54, M	8/10	D/E	spastic, para		T3–4	lateral	T3–4			2.1
16	73, M	6/7	C/D	flaccid, para	OPLL C2–4, T3–5	T11–12	tuberous	T11–12			3.0
17	67, M	7/8	C/D	spastic, para		T8–11	enlarged	T7–11			8.1
18	62, M	8/8	D/D	spastic, para	OPLL C5–6	T10–11	enlarged	T10–11			7.2
19	57, M	5/6	C/C	spastic, para	OPLL C3–1, T4–6	T4–5	fused	T2–5			6.8
20	67, F	6/9	D/E	spastic, para	OPLL C3–6, T8–11	T3–4	enlarged	T3–4			3.0
21	62, M	6/9	C–E	spastic, para	OPLL C4–6	T3–5	enlarged	T3–6			5.2
22	47, F	8/8	D–D	flaccid, para	OPLL T5–6	T10–12	tuberous	T10–12	dura mater ossification		5.5
23	56, M	8/10	D–E	spastic, para		T9–12	lateral	T9–12			2.0
24	56, M	9/10	E–E	flaccid, mono		T10–12	tuberous	T10–12	dura mater ossification		3.4
25	70, F	4/7	C–D	spastic, para		T9–11	extended	T9–11			5.0
26	50, F	6/8	C–D	spastic, para	OPLL T3–7	T4–6	enlarged	T3–8			4.7
27	71, M	9/10	E–E	flaccid, mono	OPLL C4–6	T11–12	lateral	T11–12			1.5
28	53, M	6/3	C–B	spastic, para	OPLL C5–6, T11–12	T11–12	fused	T11–12	circumspinal decompression	transient SCI	4.5
29	73, F	5/8	C–E	spastic, para		T9–11	enlarged	T10–11			2.6
30	53, F	7/7	D–D	spastic, para		T8–9	fused	T8–9			3.0
31	72, M	4/7	C–D	flaccid, para		T9–11	enlarged	T9–11			2.0
32	70, M	8/9	D–E	flaccid, para		T11–12	enlarged	T11–12			1.0
33	63, F	7/9	C–E	spastic, para		T10–11	fused	T10–11			2.0
34	77, M	5/7	C–D	flaccid, para		T12–L1	extend	T12–L2			1.5
35	76, M	5/8	C–E	flaccid, para		T11–12	fused	T11–12			1.5
36	73, F	5/7	D–D	flaccid, para		T10–11	tuberous	T10–12			1.3
37	63, F	6/8	D–D	flaccid, para		T10–L1	fused	T10–12			1.0
38	67, F	7/10	D–E	spastic, para		T5–6	lateral	T5–6			1.2
39	54, M	8/11	D–E	spastic, para		T11–12	enlarged	T11–12			0.6
40	76, F	6/3	D–B	spastic, para	OPLL T3–7	T4–6	fused	T4–6	circumspinal decompression	transient SCI	0.9
41	71, F	5/6	C–D	spastic, para	OPLL C3–T2, T8–9	T8–9	extended	T8–9	pedicular screwing		0.8
42	62, F	6/8	C–E	spastic, para	OPLL C4–6	T10–11	enlarged	T10–11			0.5
43	68, M	7/9	D–E	spastic, epiconus		T10–11	extended	T10–11			0.5

* ASIA = American Spinal Injury Association; B-S = Brown–Séquard syndrome; FU = follow-up; mono = monoparesis; para = paraparesis; SCI = spinal cord injury.

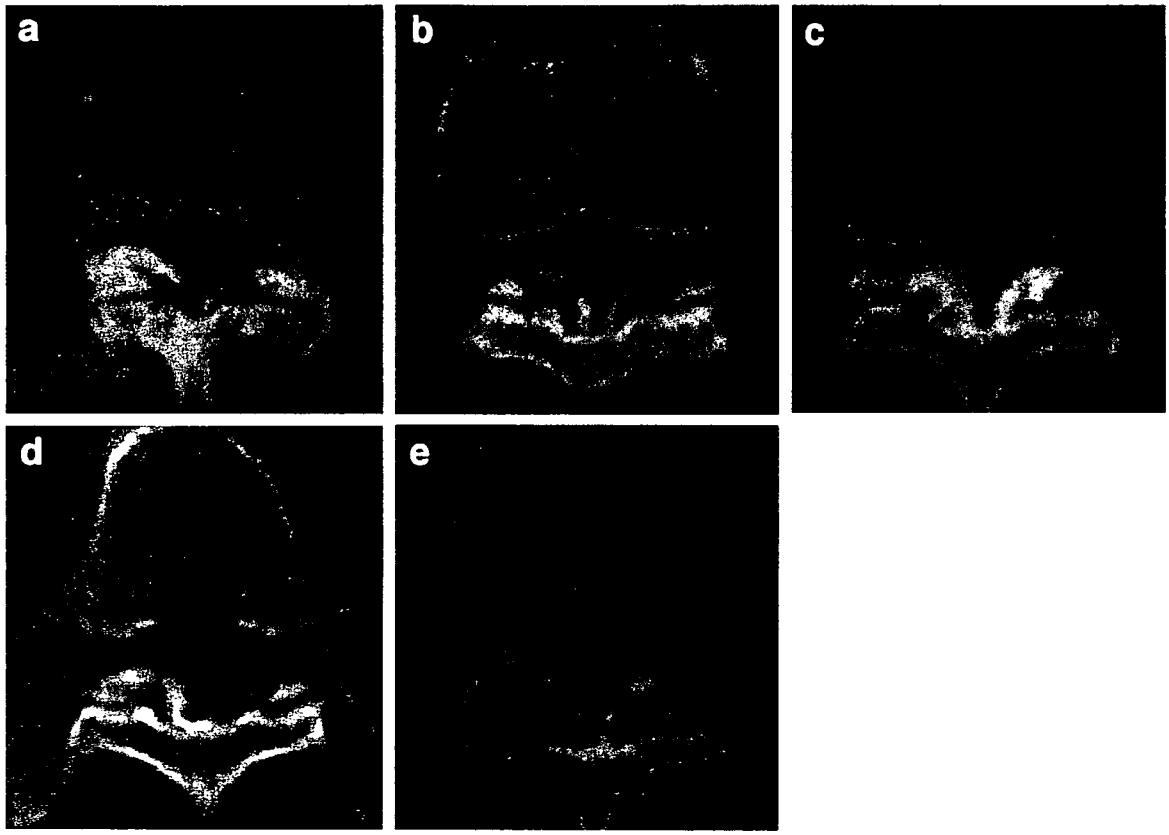

FIG. 1. Computed tomography scans demonstrating lateral (a), extended (b), enlarged (c), fused (d), and tuberous (e) types of OLF.

ists in bone and cartilage pathology (K.U., Y.K.), who were not involved in the histopathological and immunohistochemical processing. Written informed consent was obtained from each patient, and the study protocol was approved by the Human Ethics Review Committee of our university.

Histopathological Processing and Immunohistochemical Staining

Details of the histopathological and immunohistochemical processing procedures have been described previously by our group.[8,38,39] The resected OLF plaque, together with the surrounding ligament and ligamentous enthesis, was bisected midsagittally and then fixed with 10% buffered formaldehyde for 48 hours at 4°C. The samples were further decalcified for 4 to 7 days at 4°C in 0.5 M ethylenediaminetetraacetic acid (0.5 M Tris-HCl buffer) at a pH of 7.6, and then embedded in paraffin using standard procedures. Serial 4-μm-thick cryostat sagittal sections of the OLF-ligament-enthesis complex were prepared for H & E, elastica van Giesen, and toluidine blue (pH 7.4) staining.

For immunohistochemical staining, serial 4-μm-thick sections were prepared from the paraffin-embedded specimens, deparaffinized with xylene, and treated with ethanol. After washing with water, the intrinsic peroxidase was blocked with 0.3% H_2O_2/methanol solution at 20°C for 10 minutes and washed with PBS (pH 7.4). The sections were placed in a polypropylene slide-holder with a cap filled with PBS and irradiated in a 200 W microwave oven three times for 5 minutes.

The sections were then reacted with a blocking solution (PBS-containing carrier protein and 15 mM sodium azide; LSAB kit, Lot 00075, Dako) at 20°C for 10 minutes. This step was followed by reaction with the following primary antibodies at 4°C overnight: monoclonal anti–type I collagen (mouse, Lot IX1229; R&D Systems); monoclonal anti–type II collagen (mouse, Lot GU1219; R&D Systems); monoclonal anti–BMP-2 (mouse, AR004, Lot UED014091, 0.2 μL filtered solution in PBS with 5% trehalose; R&D Systems); monoclonal anti-TGFβ (mouse, MAB1835, Lot CCI021021, 0.2 μL filtered solution in PBS; R&D Systems); and monoclonal anti-VEGF (mouse, SC7269, Lot G231T, 200 μg dissolved in 1 ml of PBS, containing 0.1% sodium azide and 0.2% gelatin; Santa Cruz Biotechnology). Sections were further reacted with goat anti–mouse immunoglobulin antibodies conjugated to peroxidase-labeled dextran polymer (DakoCytomation EnVision System; Dako) at 20°C for 45 minutes and rinsed with PBS at a pH of 7.4. To visualize the peroxidase color reaction, sections were incubated with 3′3-diaminobenzidine/HCl solution (CB090, 50 mg dissolved in 100 ml of 0.05 M Tris-HCl buffer at a pH of 7.4; Dojin Chemicals) at 20°C for 10 minutes, and washed in water. Nuclear counterstaining was performed using hematoxylin.

Results

Clinical Presentation and Neurological Outcome

The demographic, clinical, and radiological data are summarized in Table 2. Forty of 43 patients improved neurologically after decompression. The T-11 vertebral level was the most commonly involved in OLF, and the T10–11 intervertebral level was most frequently decompressed. Computed tomography helped identify the lateral type of OLF in six patients, extended in six, enlarged in 11, fused in 13, and tuberous in seven patients. There was no correlation between the level involved and the CT classification of lesion type. In four patients, the dura was also ossified. Based on the CT findings, all four cases were classified as tuberous. Three cases (one tuberous type and two fused

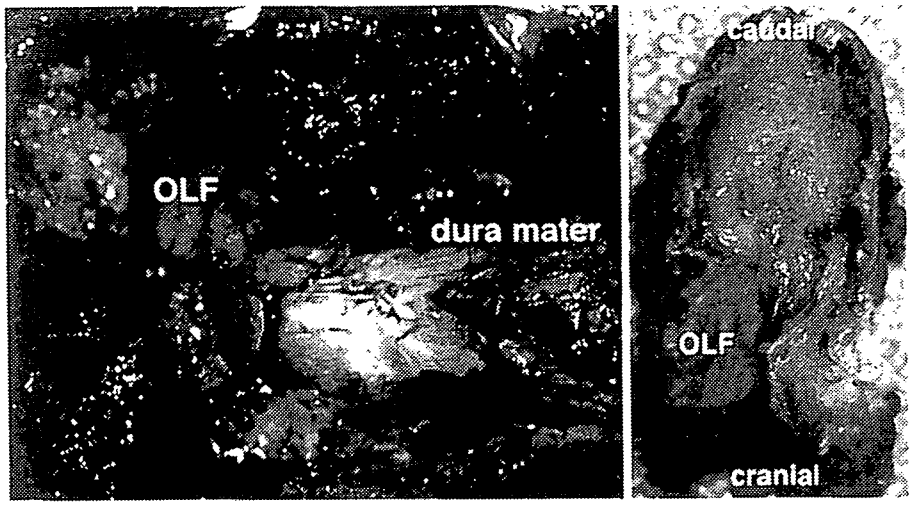

FIG. 2. Case 36. This intraoperative photograph *(left)* shows the ossified lesion carefully pulled away from the dura mater following microdissection of the adherent tissue. The photograph of the resected sample *(right)* shows the aspect of the sample that faced the dura.

types) showed neurological worsening after surgery despite the absence of any acute abnormality (amplitude decrement and/or the latency delay of the N1 spike) in spinal cord evoked potentials; unintended and minor technical insults to the already damaged spinal cord were blamed for neurological deterioration in these three cases with advanced ossification.

Histopathological Findings

The macroscopic view of the dural aspect of the yellowish-white OLF sample resected en bloc showed a regionally round, or semioval, hard protrusion toward the spinal canal with a relatively smooth surface (Fig. 2 *right*).

Photomicrographs of the specimens showed that ligamentous ossification appeared to commence at the superior margin of the lamina. Elastic fibers of the ligamentum flavum, in both insertions (caudal and cephalad lamina), extended to the laminar bone through the fibrocartilage layer, calcification front, and calcified cartilage layer, in that order. In the lateral type of OLF, the calcification front was disordered and the elastic fiber bundle became partially disorganized (Fig. 3a, e, and i). In the extended type of OLF, the calcification front spread widely along with the elastic fiber bundles, and these fibers were found to be more irregularly arranged with thinning in their diameters (Fig. 3b, f, and j). On the other hand, in the enlarged type of OLF, significant changes in the calcification front, elastic fiber bundles, and chondrocytes were observed (Fig. 3c, g, and k). The calcification front was wider than in the lateral and enlarged types of OLF, and became more irregularly woven. The elastic fiber bundles showed marked fragmentation and disappearance in the calcification front, and in the ligamentous area near the calcification front. In addition, a significant number of chondrocytes was found around the calcification front. Marked changes were also observed in the fused and tuberous types of OLF (Fig. 3d, h, and l). The calcification front showed significant irregularity together with several disruptions. This irregularity in the calcification front extended not only along the longitudinal direction of the elastic fibers, but also toward the other directions. The elastic fibers disappeared completely around the area of the calcification front. Chondrocytes were arranged in an orderly fashion along the lines where the elastic fibers were located.

Immunohistochemical Findings

Expression of Type I and II Collagens. Expression of type I collagen was qualitatively significant in the ossified area (Fig. 4 *left column*). Expression of type II collagen was rather significant in the calcified cartilage layer and in the fibrocartilage layer (Fig. 4 *right column*). In the enlarged, fused, and tuberous types of OLF, the expression levels of these collagens were more significant (qualitatively) than in the lateral type, although no quantitative assessment was performed.

Expression of BMP-2 and TGFβ. Marked expression of BMP-2 and TGFβ was noted in the calcified cartilage and fibrocartilage layers. This expression was mainly found in the cytoplasm of hypertrophic chondrocytes in these layers, rather than in the fiber area (Fig. 5, *left and middle columns*). The expression of TGFβ was negative in the fiber area near the fibrocartilage layer (Fig. 5h). A large number of BMP-2-positive or TGFβ-positive chondrocytes were found around the calcification front. A number of BMP-2-positive fibroblasts were also observed in the fiber area near the calcified and ossified areas (Fig. 5g).

Expression of VEGF. A number of VEGF-positive chondrocytes were identified in the calcified cartilage and fibrocartilage layers. Fibroblasts in the ligament were negative for VEGF staining (Fig. 5c, f, and i).

Discussion

Ossification of the ligamentum flavum often occurs in the thoracic spine,[14,16,20,24,25] whereas OPLL is frequently noted in the cervical spine.[7,22,33] The ligamentum flavum of the thoracic spine is persistently subjected to distraction

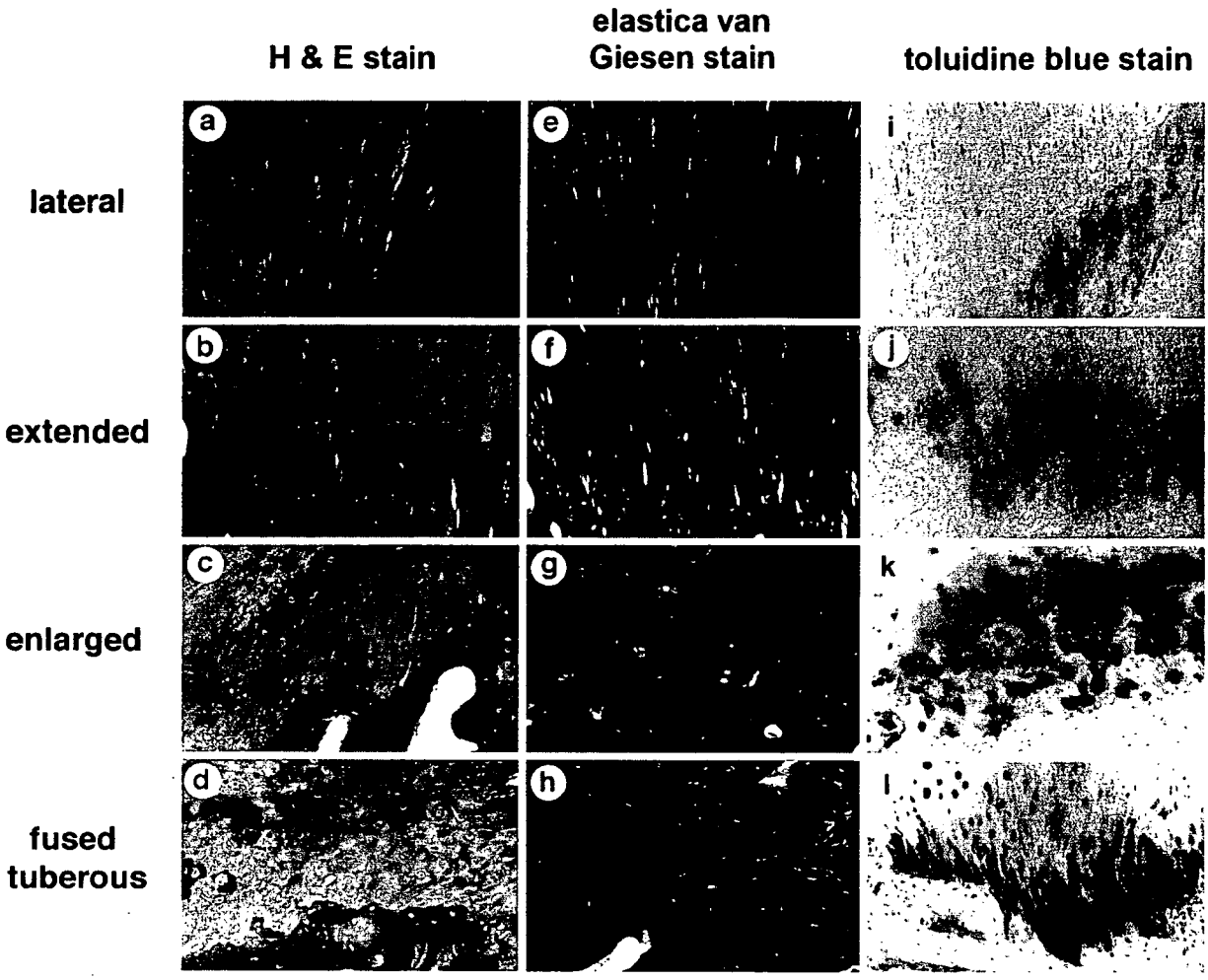

FIG. 3. Photomicrographs show the histopathological findings in various types of OLF using three different stains. The calcification front was disordered, and the elastic fiber bundle became partially disorganized in the lateral type (Case 27). In the extended type (Case 25), the calcification front spread widely along with the elastic fiber bundles, and these fibers were more irregularly arranged with thinning in their extended diameters. In the enlarged type (Case 29), the calcification front was wider than in the lateral and extended types of OLF and became more irregularly woven. Elastic fiber bundles showed marked fragmentation and disappearance in the calcification front and in the ligamentous area near the calcification front. A significant number of chondrocytes was found around the calcification front. In the fused and tuberous types (both types showed similar features; Case 35), the calcification front showed significant irregularity together with several disruptions, and this irregularity extended not only along the longitudinal direction of the elastic fibers, but also in other directions. Elastic fibers disappeared completely around the area of the calcification front, and chondrocytes were arranged in an orderly fashion along the lines where the elastic fibers were located. Original magnification × 10.

stress along its longitudinal axis, together with large mechanical overload. Perhaps as Li and colleagues[15] recently noted, mechanical axial overload and subsequent increased tensile stress applied to the thoracic ligamentum flavum may facilitate the ossification process. It is possible that this mechanical tensile stress results in the transformation of elastic fibers into ossified tissue, probably involving genetic cellular properties as well as undifferentiated mesenchymal cells.

Reviewing the current patient series, we were unfortunately unable to extract new information regarding the characteristics of level-specific prevalence, sex, and neurological severity of OLF. Using fluorine-18–labeled fluorodeoxyglucose–positron emission tomography, we compared the clinicopathological features of ossification of the posterior longitudinal ligament of the cervical spine with those of large ossified plaques (such as fused types or tuberous types).[34] Our results showed that the latter tended to be associated with neurological complications; however, there was no significant relationship between progression of ossification and magnitude of neurological impairment. This result may be explained simply by the site of the OLF lesion, located posteriorly to the spinal cord exhibiting kyphotic alignment. In addition, the OLF lesion is far from the anterior grey horn; the thoracic spinal cord, which is always subjected to some longitudinal tensile stress, is more susceptible to mechanical and neurological damage from anterior impingement than from the posterior com-

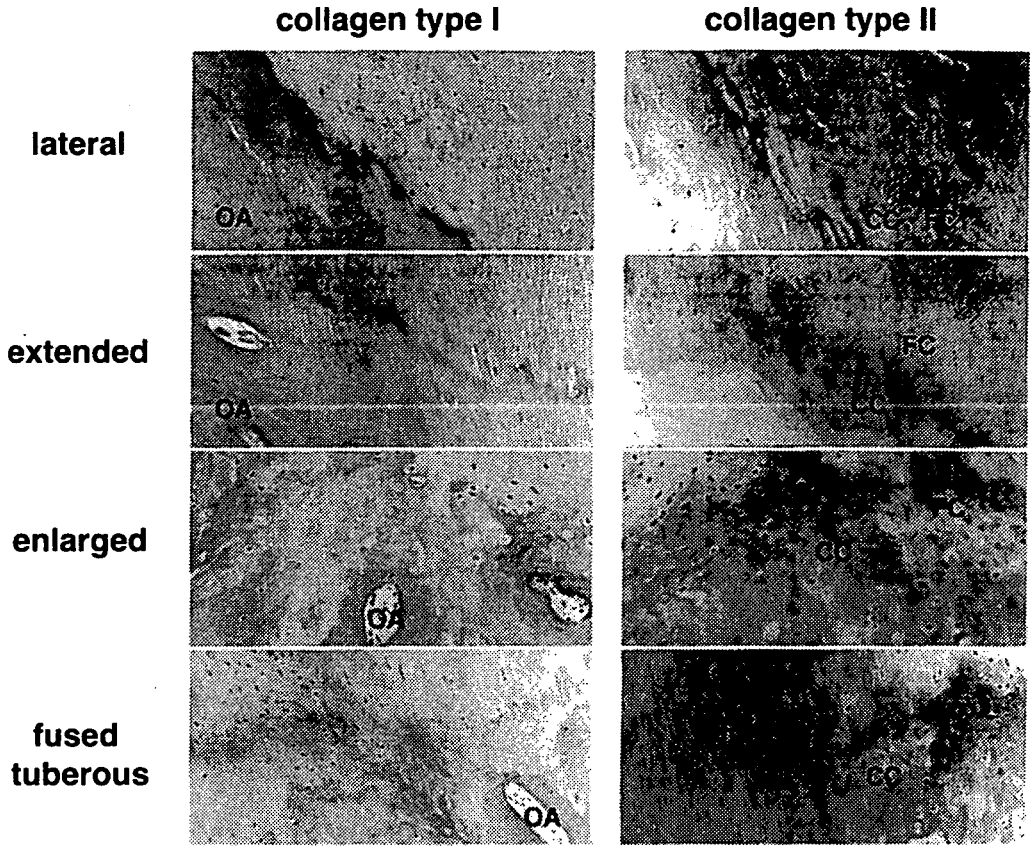

FIG. 4. Photomicrographs showing the immunostaining results for type I and type II collagens in various types (lateral, extended, enlarged, and fused and tuberous) of OLF. The expression of type I collagen was qualitatively significant in the ossified area (OA). The expression of type II collagen was significant in the calcified cartilage layer (CC) and fibrocartilage layer (FC). Original magnification × 10.

pression of OLF.[31] In spite of multisegmental involvement of the vertebrae, the levels responsible for myelopathy are limited to two to three interlaminar levels, resulting in a spinal cord "funnel-shape" deformity.[5] In four patients (9.3%) in this series, ossification was found in the dura as well as in the neighboring OLF lesion. This ossification process was probably due to dilution of cytokines related to osteogenesis (such as BMP-2, TGFβ_1, and interleukin-1β) from the ligamentum flavum during the process of ossification. Accumulation of more samples of ossified dura would allow investigation of this issue in greater detail.

The authors of several studies[13,19] have examined the histopathological and ultrastructural abnormalities of thoracic OLF. These investigators reported that infiltration of fibroblast-like mesenchymal cells into the ligamentum flavum, as well as fibroblasts within the nonossified cartilaginous cartilage, was mediated by TGFβ_1. These researchers concluded that overexpression of cytokines or peptides around the calcification and ossification fronts plays a role in the pathogenesis of OLF. In the present study, coarse disorganization of the elastic fibers was found in the ligamentum flavum around the ossified lesion, similar to the findings in calcium crystal deposition,[38,39] and more interestingly, the findings appeared more significant in fused and tuberous types of OLF than in the lateral and extended types. The calcification and ossification fronts were adjacent to the ossified lesion in the lateral type of OLF, markedly extended toward the noncalcified fibrocartilage areas along the fiber direction in the enlarged type of OLF, and irregularly crossed each other in the fused type of OLF. We also found abundant osteoblast-like cells, presumably mesenchymal cells that were metaplastic, within and around the calcification front, mainly in the fused and tuberous types of OLF compared with the lateral and extended types of OLF. These data could be interpreted as essentially different patterns of expression of osteogenetic or bone-inducing cytokines in the ligament near the already ossified area. Our group[4,8] has previously reported similar findings of infiltration of mesenchymal chondroblast- or osteoblast-like cells within the disorganized and torn elastic fibers in the posterior longitudinal ligament in the spinal hyperostotic mouse (twy/twy). Considered together, these results point to a common molecular mechanism, but the peptides or cellular responses that mediate the ossification process in the nonossified ligament remain to be studied.

Expression of type I collagen was significant in the ossified lesion site, whereas expression of type II collagen was marked in chondroblast-like cells and hypertrophied chondrocytes in the ossification front and in the ligament near the ossified lesion. It is possible that similar events could also occur in early-stage thoracic OLF in humans. Based on the present results, we are currently using immunohisto-

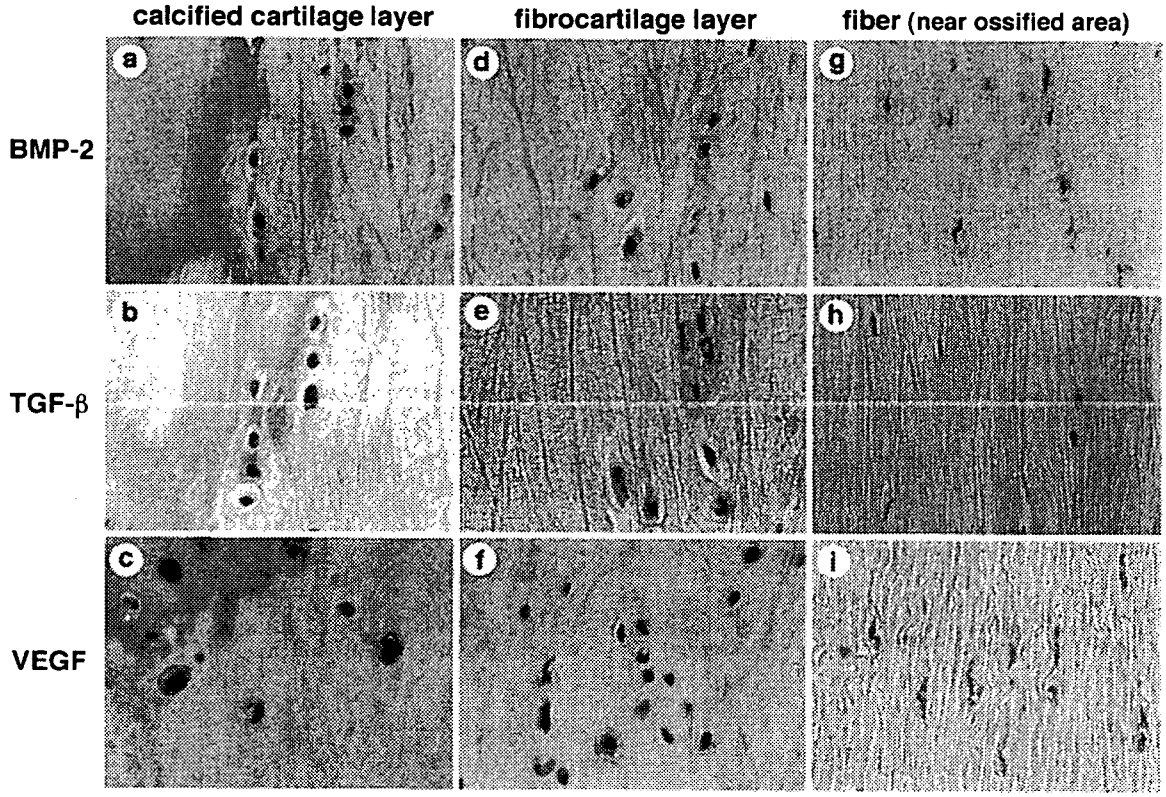

FIG. 5. Photomicrographs showing the immunostaining results for BMP-2, TGFβ, and VEGF in the calcified cartilage layer (a–c), fibrocartilage layer (d–f), and fiber (near the ossified area, g–i). Marked expression of BMP-2 and TGFβ was noted in both the calcified cartilage and fibrocartilage layers (a, b, d, and e), mainly in the cytoplasm of hypertrophic chondrocytes in these layers, rather than in the fiber area (g and h). The expression of TGFβ was negative in the fiber area (h). A number of BMP-2–positive fibroblasts were also observed in the fiber area near the calcified and ossified areas (g). A number of VEGF-positive chondrocytes were identified in the calcified cartilage and fibrocartilage layers (c and f). Fibroblasts in the ligament were negative for VEGF staining (i). Original magnification × 20.

chemical techniques to examine the process responsible for the appearance of mesenchymal fibroblasts and proliferating metaplastic hypertrophic chondrocytes at sites near the ossified lesion, as well as the subsequent ossification process. In the spinal hyperostotic mouse (twy/twy) model, in which mice develop spontaneous ossification/calcification of the cervical spine, our group[4,8,39] indicated the existence of proliferating cell nuclear antigen–positive primitive mesenchymal cells within the degenerated elastic fibers of the ligament, together with revascularization and biochemical changes in the extracellular matrix. These primitive cells were positive for S100 protein and alkaline phosphatase and the matrix was positive for chondroitin-4-sulfate proteoglycan. A number of small matrix vesicles containing calcium phosphate crystals appeared in the stroma of the degenerated spinal ligament tissue.[12] Based on these findings, we speculated that the alkaline phosphatase–positive osteoblast-like cells within the degenerated ligament, particularly in the ligamentous enthesis, might enhance enchondral ossification in the matrix. On the other hand, Iwamoto and colleagues[12] and Tsukamoto and coworkers[30] indicated that application of cyclic mechanical distraction stress to the coccygeal vertebrae of rats resulted in hypertrophy of the posterior longitudinal ligament, which was associated with infiltration of a large number of round chondrocyte-like cells within the ligamentous tissue. These chondrocyte-like cells were positive for S100 protein and Sox9, a transcription factor that activates both chondrocyte differentiation and cartilage formation, and were believed to produce matrix protein enriched with glycosaminoglycans. These investigators concluded that elastic fibers in the spinal ligament (posterior longitudinal ligament and ligamentum flavum) are sensitive to repetitive cyclic stretch stress and that under such stress, mesenchymal fibroblastic cells transform to chondrocytes and osteoblasts in association with increased expression of BMP-2, TGFβ$_1$, and Sox9. We observed a number of hypertrophied chondrocytes in the ossified lesions, which were positive for these cytokines, within the stroma near the ossification front together with neovascularization, which suggests that they play important roles in the ossification process.

Conclusions

We observed significant degeneration of elastic fibers in both the caudal and proximal parts of the ligamentum flavum. A coarse arrangement of often fragmented and hyper-

trophied elastic fibers was marked in the nonossified area of the ligamentum flavum near its origin and attachment. In addition, a number of chondrocytes or chondroblast-like cells of variable size appeared in the stroma of the degenerated ligament in association with ligament degeneration. These cells were positive for TGFβ and BMP-2, and the findings were more significant in the area adjacent to calcification and ossification.

References

1. Aizawa T, Sato T, Sasaki H, Kusakabe T, Morozumi N, Kokubun S: Thoracic myelopathy caused by ossification of the ligamentum flavum: clinical features and surgical results in the Japanese population. **J Neurosurg Spine 5:**514–519, 2006
2. Al-Orainy IA, Kolawole T: Ossification of the ligament flavum. **Eur J Radiol 29:**76–82, 1998
3. Arafat QW, Jackowski A, Chavda SV, West RJ: Case report: ossification of the thoracic ligamenta flava in a Caucasian: a rare cause of myelopathy. **Br J Radiol 66:**1193–1196, 1993
4. Baba H, Furusawa N, Fukuda M, Maezawa Y, Imura S, Kawahara N, et al: Potential role of streptozotocin in enhancing ossification of the posterior longitudinal ligament of the cervical spine in the hereditary spinal hyperostotic mouse *(twy/twy)*. **Eur J Histochem 41:**191–202, 1997
5. Baba H, Tomita K, Kawahara N, Kikuchi Y, Imura S: Spinal cord evoked potentials in thoracic myelopathy with multisegmental vertebral involvement. **Spine 17:**1291–1295, 1992
6. Ben Hamouda K, Jemel H, Haouet S, Khaldi M: Thoracic myelopathy caused by ossification of the ligamentum flavum: a report of 18 cases. **J Neurosurg 99 (2 Suppl):**157–161, 2003
7. Epstein NE: Ossification of the yellow ligament and spondylosis and/or ossification of the posterior longitudinal ligament of the thoracic and lumbar spine. **J Spinal Disord 12:**250–256, 1999
8. Furusawa N, Baba H, Imura S, Fukuda M: Characteristics and mechanism of the ossification of posterior longitudinal ligament in the tip-toe walking Yoshimura (twy) mouse. **Eur J Histochem 40:**199–210, 1996
9. He S, Hussain N, Li S, Hou T: Clinical and prognostic analysis of ossified ligamentum flavum in a Chinese population. **J Neurosurg Spine 3:**348–354, 2005
10. Ishida Y, Kawai S: Characterization of cultured cells derived from ossification of the posterior longitudinal ligament of the spine. **Bone 14:**85–91, 1993
11. Ishida Y, Kawai S: Effects of bone-seeking hormones on DNA synthesis, cyclic AMP level, and alkaline phosphatase activity in cultured cells from human posterior longitudinal ligament of the spine. **J Bone Miner Res 8:**1291–1300, 1993
12. Iwamoto Y, Tsukamoto N, Maeda K, Mira H, Hosokawa T, Harimaya K, et al: [Effects of repetitive distraction stress on rat spinal ligaments: in vivo cell biological study.] **Annual Report of Researches on Ossification of the Spinal Ligament 18:**65–70, 2006 (Jpn)
13. Kawaguchi H, Kurokawa T, Hoshino Y, Kawahara H, Ogata E, Matsumoto T: Immunohistochemical demonstration of bone morphogenetic protein-2 and transforming growth factor-beta in the ossification of the posterior longitudinal ligament of the cervical spine. **Spine 17 (3 Suppl):**S33–S36, 1992
14. Kruse JJ, Awasthi D, Harris M, Waguespack A: Ossification of the ligamentum flavum as a cause of myelopathy in North America: report of three cases. **J Spinal Disord 13:**22–25, 2000
15. Li F, Chen Q, Xu K: Surgical treatment of 40 patients with thoracic ossification of the ligamentum flavum. **J Neurosurg Spine 4:**191–197, 2006
16. Li KK, Chung OM, Chang YP, So YC: Myelopathy caused by ossification of ligamentum flavum. **Spine 27:**E308–E312, 2002
17. Liao CC, Chen TY, Jung SM, Chen LR: Surgical experience with symptomatic thoracic ossification of the ligamentum flavum. **J Neurosurg Spine 2:**34–39, 2005
18. Miyakoshi N, Shimada Y, Suzuki T, Hongo M, Kasukawa Y, Okada K, et al: Factors related to long-term outcome after decompressive surgery for ossification of the ligamentum flavum of the thoracic spine. **J Neurosurg 99 (3 Suppl):**251–256, 2003
19. Miyamoto S, Yonenobu K, Ono K: [Immunohistochemical demonstration of transforming growth factor-beta, fibronectin, and alkaline phosphatase in cellular proliferation of ossification of the spinal ligaments.] **Spine Spinal Cord 6:**803–813, 1993 (Jpn)
20. Okada K, Oka S, Tohge K, Ono K, Yonenobu K, Hosoya T: Thoracic myelopathy caused by ossification of the ligamentum flavum. Clinicopathologic study and surgical treatment. **Spine 16:** 280–287, 1991
21. Polgär F: Über interarkuelle Wirbelverkalkung. **Fortschr Geb Rontgenstr Nuklearmed Erganzungsband 40:**292–298, 1920
22. Sakou T, Taketomi E, Matsunaga S, Yamaguchi M, Sonoda S, Yashiki S: Genetic study of ossification of the posterior longitudinal ligament in the cervical spine with human leucocyte antigen haplotype. **Spine 16:**1249–1252, 1991
23. Sato T, Kokubun S, Tanaka Y, Ishii Y: Thoracic myelopathy in the Japanese: epidemiological and clinical observations on the cases in Miyagi Prefecture. **Tohoku J Exp Med 184:**1–11, 1998
24. Seichi A, Nakajima S, Takeshita K, Kitagawa T, Akune T, Kawaguchi H, et al: Image-guided resection for thoracic ossification of the ligamentum flavum. **J Neurosurg 99 (1 Suppl):**60–63, 2003
25. Shiokawa K, Hanakita J, Suwa H, Saiki M, Oda M, Kajiwara M: Clinical analysis and prognostic study of ossified ligamentum flavum of the thoracic spine. **J Neurosurg 94 (2 Suppl):**221–226, 2001
26. Tanaka T, Ikari K, Furushima K, Okada A, Tanaka H, Furukawa K, et al: Genomewide linkage and linkage disequilibrium analyses identify *COL6A1*, on chromosome 21, as the locus for ossification of the posterior longitudinal ligament of the spine. **Am J Hum Genet 73:**812–822, 2003
27. Tanaka Y, Sato T, Aizawa T: Surgery for ossification of the ligamentum flavum, in Yonenobu K, Nakamura K, Toyama Y (eds): **OPLL: Ossification of the Posterior Longitudinal Ligament, ed 2.** Tokyo: Springer, 2006, pp 265–269
28. Terakado A, Tagawa M, Goto S, Yamazaki M, Moriya H, Fujimura S: Elevation of alkaline phosphate activity induced by parathyroid hormone in osteoblast-like cells from the spinal hyperostotic mouse TWY *(twy/twy)*. **Calcif Tissue Int 56:** 135–139, 1995
29. Tomita K, Kawahara N, Baba H, Kikuchi Y, Nishimura H: Circumspinal decompression for thoracic myelopathy due to combined ossification of the posterior longitudinal ligament and ligamentum flavum. **Spine 15:**1114–1120, 1990
30. Tsukamoto N, Maeda T, Miura H, Jingushi S, Hosokawa A, Harimaya K, et al: Repetitive tensile stress to rat caudal vertebrae inducing cartilage formation in the spinal ligaments: a possible role of mechanical stress in the development of ossification of the spinal ligaments. **J Neurosurg Spine 5:**234–242, 2006
31. Uchida K, Baba H, Maezawa Y, Furukawa S, Furusawa N, Imura S: Histological investigation of spinal cord lesions in the spinal hyperostotic mouse *(twy/twy)*: morphological changes in anterior horn cells and immunoreactivity to neurotropic factors. **J Neurol 245:**781–793, 1998
32. Uchida K, Baba H, Maezawa Y, Kubota C: Progressive changes in neurofilament proteins and growth-associated protein-43 immunoreactivities at the site of cervical spinal cord compression in spinal hyperostotic mice. **Spine 27:**480–486, 2002
33. Uchida K, Kobayashi S, Nakajima H, Kokubo Y, Yayama T, Sato R, et al: Anterior expandable strut cage replacement for osteoporotic thoracolumbar vertebral collapse. **J Neurosurg Spine 4:** 454–462, 2006
34. Uchida K, Kobayashi S, Yayama T, Kokubo Y, Nakajima H, Kakuyama M, et al: Metabolic neuroimaging of the cervical spi-

nal cord in patients with compressive myelopathy: a high-resolution positron emission tomography study. **J Neurosurg Spine 1:** 72–79, 2004
35. Vasudevan A, Knuckey NW: Ossification of the ligamentum flavum. **J Clin Neurosci 9:**311–313, 2002
36. Yamamoto Y, Furukawa K, Ueyama K, Nakanishi T, Takigawa M, Harata S: Possible roles of CTGF/Hcs24 in the initiation and development of ossification of the posterior longitudinal ligament. **Spine 27:**1852–1857, 2002
37. Yamazaki M, Goto S, Kobayashi Y, Terakado A, Moriya H: Bone cells from spinal hyperostotic mouse *(twy/twy)* maintain elevated levels of collagen production in vitro. **J Bone Miner Metab 12:** 57–63, 1994
38. Yayama T, Baba H, Furusawa N, Kobayashi S, Uchida K, Kokubo Y, et al: Pathogenesis of calcium crystal deposition in the ligamentum flavum correlates with lumbar spinal canal stenosis. **Clin Exp Rheumatol 23:**637–643, 2005
39. Yayama T, Furusawa N, Baba H, Kokubo Y, Yoshizawa K, Fukuda M: Calcium crystal deposition in the ligamentum flavum of the lumbar spine: role of sex hormones and transforming growth factorβ. **Acta Histochem Cytochem 36:**83–91, 2003

Manuscript submitted November 21, 2006.
Accepted April 10, 2007.
This work was supported in part by grants from the Investigation Committee on Ossification of the Spinal Ligaments, the Public Health Bureau of the Japanese Ministry of Health and Welfare, and by Grants-in-Aid for General Scientific Research (No. 16390435 and No. 18390411) offered by the Japanese Ministry of Education, Science, and Culture.

Address reprint requests to: Takafumi Yayama, M.D, D.M.Sc., Matsuokashimoaizuki 23, Eiheiji, Fukui 910–1193, Japan. email: yayama@fmsrsa.fukui-med.ac.jp.

JOURNAL OF NEUROTRAUMA
Volume 24, Number 4, 2007

Pp. 703–712
DOI: 10.1089/neu.2006.0004

Rescue of Rat Anterior Horn Neurons after Spinal Cord Injury by Retrograde Transfection of Adenovirus Vector Carrying Brain-Derived Neurotrophic Factor Gene

***HIDEAKI NAKAJIMA, *KENZO UCHIDA, SHIGERU KOBAYASHI, TOMOO INUKAI, YUKIKO HORIUCHI, TAKAFUMI YAYAMA, RYUICHIRO SATO, and HISATOSHI BABA**

ABSTRACT

We investigated the efficacy of retrograde gene delivery via the sternomastoid muscle of recombinant adenovirus vector (AdV) carrying brain-derived neurotrophic factor (BDNF) gene for the rescue of injured rat spinal cord. One hundred-thirty five adult Sprague-Dawley rats were used in the study with a standard weight-compression technique to produce spinal cord injury. AdV-BDNF gene or AdV-β-galactosidase (AdV-LacZ) gene was injected into the sternomastoid muscle immediately after traumatic C4 segment spinal cord injury. AdV-BDNF was successfully appeared in the injured cervical spinal cord following injection into the sternomastoid muscle. BDNF expression in the anterior horn neurons of the cervical spinal cord reached peak levels at 1–2 weeks; and the expression persisted at significant levels for approximately 4 weeks after injury. AdV-BDNF transfection was associated with increased numbers of intact neurons as confirmed by Nissl, cholineacetyltransferase (ChAT), and acetylcholine esterase (AChE) staining especially from 2 weeks after injury, compared with the AdV-LacZ injected rats. Our results suggest that *in vivo* targeted retrograde AdV-BDNF-gene delivery may enhance neuronal survival following traumatic injury of the spinal cord.

Key words: axonal transport; growth factor; regeneration; spinal cord injury; therapeutic approaches for the treatment of CNS injury; traumatic spinal cord injury

INTRODUCTION

THE INITIAL MECHANICAL DAMAGE after spinal cord injury is followed by a cascade of potentially harmful secondary events that include posttraumatic ischemia, formation of free radicals, detrimental inflammatory responses, and death of neuron and glial cells (Nakahara et al., 1999; Blesch et al., 2002). Although most functional deficits reflect the interruption of axonal pathway in the white matter, motoneuron loss is also associated with permanent locomotion impairment after spinal cord injury. Rescue of motoneurons from injury-induced death is an important prerequisite for muscle reinnervation, as was demonstrated in the case of cervical spinal cord injury that caused serious arm motor deficit (Collazos-Castro et al., 2005). A number of experimental studies have at-

*These two authors contributed equally to this work.
Division of Orthopaedics and Rehabilitation Medicine, Department of Surgery, University of Fukui Faculty of Medical Sciences, Fukui, Japan.

tempted to establish a feasible method for improvement of the spinal cord function after neural injury. For example, neuronal (McDonald et al., 1999; Blesch et al., 2002) or embryonic (Pittenger et al., 1999) stem cell transplantation, and differentiation of neurogenic progenitor cells to neurons (Ogawa et al., 2002) could enhance spinal cord regeneration (Blits et al., 2002). However, spinal cord regeneration is difficult by each transplantation alone due to the presence of a network of complex factors, and it is important to regulate first the host microenvironment. Thus, there is a need for other methods of long-term supplementation and improvement of the efficiency of localized neurotrophic factor production into the injured spinal cord.

Using a spinal hyperstotic mouse model (*twy/twy*), we demonstrated in a series of studies the important roles of brain-derived neurotrophic factor (BDNF) and neurotrophin (NT)–3 in the survival of spinal cord motoneurons, after mechanical injury of the cord (Baba et al., 1997; Uchida et al., 1998, 2002, 2003). In the adult rats injured spinal cord, BDNF expression increased transiently at 1 day and then rapidly declined to the native level at 2–3 days after injury. Neurotrophin deficiency after spinal cord injury results in a devastating sequence of events for neurons, including neuronal cell death (Nakamura and Bregman, 2001). Appropriate supplementation of neurotrophins is necessary and effective for neuronal survival (Kishino and Nakayama, 2003), and their efficacy has been reported in the field of regenerative research in damaged spinal cords (Hendriks et al., 2004; Liudmila et al., 2002). However, effective administration of neurotropins into injured spinal cord tissue remains a major challenge. Oral or systemic delivery of these neuropeptides is not practical due to the very short relapsing time and failure to pass the blood-brain and spinal cord barrier (Emborg and Kordower, 2001). These limitations of protein-based therapeutics have resulted in the development of direct administration methods of gene transduction to the nervous system by intrathecal, intracerebroventricular or intraparenchymal infusion (Mannes et al., 1998). These direct routes of neuroprotectant gene administration have been used for effective and sustainable gene delivery, but there are difficulties and serious concerns regarding the possible spread of resultant traumatic neural injury and accumulation of neural damage that may lead to further tissue damage, including necrosis, apoptosis, and cell death (Boulis et al., 2002; Keir et al., 1995; Thomas et al., 2001).

In contrast, targeted retrograde gene delivery through the peripheral nerves or muscle injection of adenovirus vectors is a less invasive method (Hendriks et al., 2004; Ruitenberg et al., 2002) with the potential for repeated administration. This approach has been used for gene delivery and treatment of injures to the central nervous system (Kuo et al., 1995; Hasse et al., 1998; Kaspar et al., 2002). However, the efficacy of retrograde gene delivery to target organs, as a possible means of cervical spinal cord injury treatment, has not been completely elucidated.

Recently, we evaluated the feasibility and efficacy of targeted retrograde gene delivery through the sternomastoid muscle (innervated by spinal accessory nerves) into the injured cervical spinal cord of rats using a recombinant adenovirus vector coding for β-galactosidase cDNA (AdV-LacZ). AdV-LacZ gene expression in the cervical spinal cord was observed from 3 days to 4 weeks after vector injection into the sternomastoid muscles. AdV-LacZ was transferred via a retrograde mechanism into the injured cervical spinal cord with high transduction efficacy (80.6–98.9%) over certain adenoviral titer and dosage (Nakajima et al., 2005). The present study is an extension to the above study, in which we evaluated the feasibility and efficacy of retrograde delivery of recombinant adenovirus vector-mediated BDNF (AdV-BDNF) gene through the sternomastoid muscle into the injured cervical spinal cord. We also discuss methodological issues related to this type of gene delivery and the neuroprotective effects on the injured spinal cord.

METHODS

Animal Model of Spinal Cord Injury

Experiments were conducted in 135 adult male Sprague-Dawley rats (Clea, Tokyo, Japan), aged 8–10 weeks with a mean body weight of 266 ± 28.2 g (mean ± standard deviation). Following anesthesia by intraperitoneal injection of sodium pentobarbiturate (0.05 mg/g body weight), laminectomy was performed at the C3 and C4 levels using a surgical microscope (VANOX-S, Olympus, Tokyo), taking utmost care in avoiding the dura mater. At the C4 segmental level, the dorsal surface of the spinal cord was compressed extradurally using a 35-g static load (custom-made rod, 2 × 3 mm in diameter) for 5 min as described previously (Black et al., 1986; Nakahara et al., 1999; Nakajima et al., 2005). After surgery, animals were housed under a 12-h light-dark cycle in a bacteria-free biologically clean room with access to food and water *ad libitum*. The experimental protocol strictly adhered to the Fukui University *Ethical Committee Guidelines for Animal Experimentation.*

Preparation of Recombinant Adenovirus Vector

The Adenovirus Expression Vector Kit (no. 6150; Takara Biomedical, Shiga, Japan) was used for recombi-

nant adenovirus production (Miyake et al., 1996). To prevent virus replication, mouse BDNF cDNA was subcloned into a cassette cosmid pAxCAwt carrying an adenovirus type-5 genome lacking the E3, E1A, and E1B regions. The cosmid pAxCAwt contains a *Swa*I cloning site flanked by a cytomegalovirus enhancer-chicken β-actin hybrid (CAG) promoter on the 5′ end and a rabbit globin poly(A) sequence on the 3′ end. The cosmid was cotransfected to 293 cells with the appropriately cleaved adenovirus DNA-terminal protein complex (COS-TPC method). The recombinant adenovirus was propagated and isolated from 293 cells and purified using two rounds of CsCl centrifugation. The control, a recombinant adenovirus vector coding for β-galactosidase cDNA (AdV-LacZ), was isolated using the same procedure. The final adenovirus vector titers contained 5.0×10^8 plaque forming units/mL. The virus vector protocol strictly followed the Fukui University *Safety Committee Guidelines for Recombinant Virus Experimentation.*

BDNF Treatment and Tissue Preparation

Table 1 summarizes the number of animals entered into the present study. Immediately after spinal cord injury, the left-sided sternomastoid muscle was exposed. Branches of the spinal accessory nerves innervating the muscles were carefully preserved. Using a microsyringe (Hamilton, Reno, NV), 100 μL of AdV-BDNF was carefully injected into the middle section of the superficial layer of the left sternomastoid muscle. In the other animals, 100 μL of AdV-LacZ was injected into the same muscle. The rats were re-anesthetized at 3 days, or 1, 2, 3, or 4 weeks later, and 300 mL of phosphate-buffered saline (PBS; at 4°C) was perfused intracardially followed by perfusion of 200 mL of 4% paraformaldehyde in 0.1 M PBS (pH 7.6). Immediately after perfusion, the spinal cord segment between the pyramidal decussation and C8 segment was removed *en bloc* and stored in 0.1 M PBS containing 20% sucrose at 4°C for 36 h. Tissue blocks were embedded in Tissue-Tek (optimal cutting temperature [OCT] compound 4583; Sakura Finetechnical, Tokyo) and stored frozen at −80°C. Fifteen uninjured rats, which underwent laminectomy and AdV-LacZ injection without compression, were also sacrificed as controls and processed as described above. Using a cryostat, serial 25-μm-thick transverse and sagittal frozen sections were prepared for BDNF immunohistochemistry ($n = 50$), and 50-μm-thick transverse frozen sections were also prepared for Nissl, cholineacetyltransferase (ChAT) and acetylcholine esterase (AChE) staining ($n = 65$). After drying at room temperature, all sections were serially mounted on glass slides and fixed with 2% paraformaldehyde in 0.1 M PBS.

Immunohistochemistry of BDNF

Serial 25-μm-thick transverse and sagittal frozen sections were treated with 0.1 M TRIS-HCl buffer (pH 7.6) containing 0.3% Triton-X-100 for another 24 h to allow reaction of the cell membrane with the antibodies. Sections were incubated for 10 minutes in Block Ace (UK-B25, Snow Brand, Tokyo) to quench endogenous peroxidase activity, and then rinsed in PBS twice for 5 min each. They were then incubated with anti-BDNF (BDNF polyclonal antibody, product no. AB1779, 1:1000; Chemicon International, Temecula, CA) diluted in PBS at 4°C overnight. Slides were then washed in PBS three times for

Table 1. Experimental Groups Used in the Present Study

	Survival period				
	3 days	*1 week*	*2 weeks*	*3 weeks*	*4 weeks*
Immunohistochemistry of BDNF after SCI (3 transverse and 2 sagittal 25 μm frozen sections)					
AdV-BDNF injected	5	5	5	5	5
AdV-LacZ injected	5	5	5	5	5
Evaluation of cervical motoneuron survival (50 μm frozen sections) by Nissl staining, ChAT immunohistochemistry, AChE histochemistry					
Uninjured AdV-LacZ injected	3	3	3	3	3
Injured AdV-BDNF injected	5	5	5	5	5
Injured AdV-LacZ injected	5	5	5	5	5
Immunoblot analysis of BDNF immunoreactivity after SCI					
AdV-BDNF injected	2	2	2	2	2
AdV-LacZ injected	2	2	2	2	2

SCI, spinal cord injury; AdV-BDNF, recombinant adenovirus vector carrying mouse brain-derived neurotrophic factor gene; AdV-LacZ, recombinant adenovirus vector coding for *Escherichia coli* β-galactosidase cDNA; ChAT, cholineacetyltransferase; AChE, acetylcholine esterase.

5 min, and sections were further incubated for 30 min with diluted biotinylated secondary antibody solution followed by washing for 5 min in PBS. The sections were again incubated for 30 min with VECTA STAIN® ABC Reagent (Vectastain Elite Kit; Vector Laboratories, Burlingame, CA) and washed for 5 min in PBS. Subsequently, sections were stained with 3,3-diaminobenzidine tetrahydrochloride (Dojin Chemicals, Tokyo) in PBS (pH 7.4) containing 0.01% H_2O_2 solution until development of the desired stain intensity, rinsed in PBS, dehydrated using graded series of ethanol, cleared in xylene, and mounted in silanized slides (no. S3003; Dako, Glostrup, Denmark) prior to being cover-slipped. These transverse sections were photomicrographed under a microscope equipped with a digital camera. The number of BDNF-positive anterior horn neurons were also counted from C1 to C8 spinal cord segments at each timepoint.

Immunoblot Analysis of BDNF in the Cervical Spinal Cord

Immunoblot analysis of BDNF expression in the injured spinal cord was performed at 3 days, and 1, 2, 3, and 4 weeks after administration of AdV-BDNF (n = 10) or AdV-LacZ (n = 10; Table 1), using the method we described previously (Uchida et al., 2003). Immediately after anesthesia, the spinal cord segment between the pyramidal decussation and C8 segment was removed *en bloc* and stored at −20°C. Sections were solubilized in RIPA buffer (50 mM pH 7.5 TRIS-HCl, 150 mM NaCl, 1% Triton X-100, 0.5% sodium deoxycholate, 20 μg/mL leupeptine, and 1 mM [phenylmethylsulfonyl fluoride (PMSF)]), homogenized and then stored at −80°C. Protein concentration was determined by a DC Protein Assay Kit (Bio-Rad Laboratories, Hercules, CA). Laemmli sodium dodecylsulfate buffer samples containing proteins were boiled and subjected to immunoblot analysis. Total protein (80 μg/lane) was subjected to sodium dodecylsulfate–polyacrylamide gel (15%) electrophoresis (SDS-PAGE) and transferred onto polyvinylidene difluoride membrane (PE Applied Biosystems, Foster, CA) for 70 min in a semi-dry blot apparatus. The membrane was washed twice in PBS containing 0.05% Tween 20, blocked by 5% skim milk in PBS for 1 h, and reacted with anti-BDNF antibody (no. AB1779, 1:1000, anti-rabbit; Chemicon International) diluted overnight at 4°C, fol-

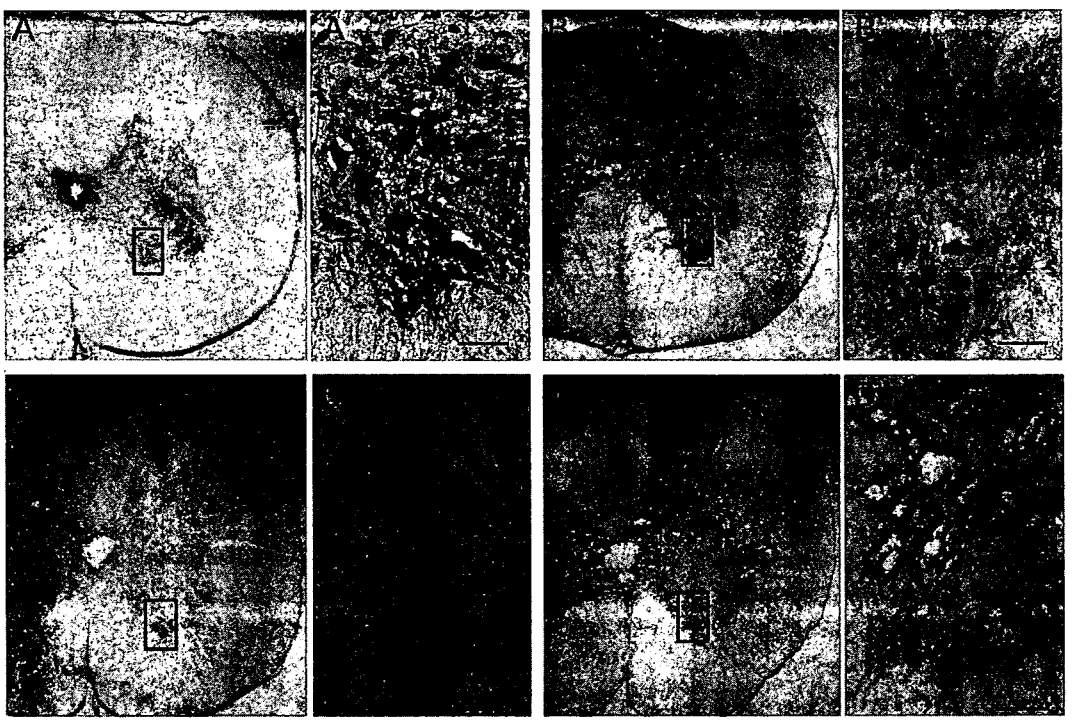

FIG. 1. Photomicrographs showing immunoreactivities for BDNF in the injured cervical spinal cord. (**A–D**) lower magnification, and (**A′–D′**) high-power photomicrograph of the box area A–D. In the transverse sections (C3 segmental level) at 1 week (A-A′, C-C′) and 4 weeks (B-B′, D-D′) after spinal cord injury, although BDNF-positive cells were observed in the AdV-BDNF injected rat (A-A′, B-B′), no BDNF-positive cells were found in AdV-LacZ injected rats (C-C′, D-D′). Original magnification, ×40 (A–D), ×200 (A′–D′). Scale bar = 100 μm (A′–D′).

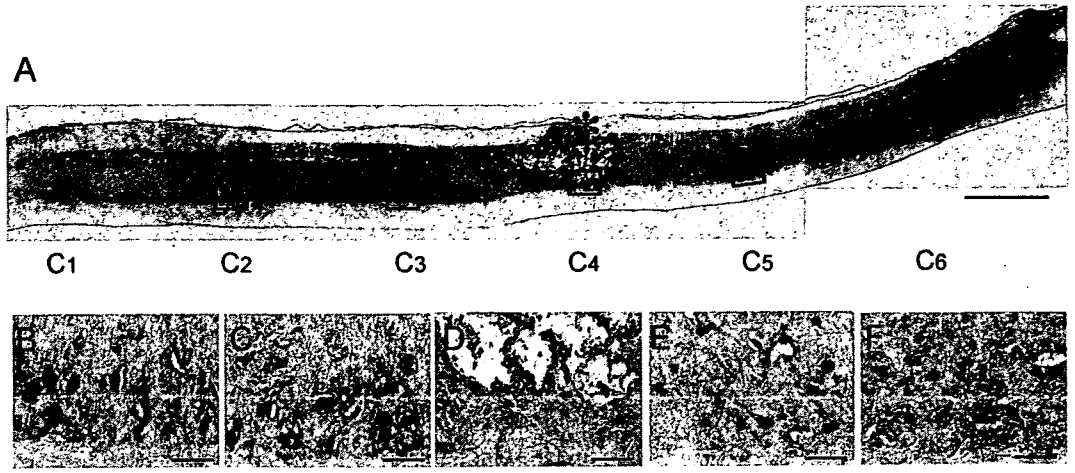

FIG. 2. Photomicrographs showing immunoreactivities for BDNF in the left-side parasagittal sections of the AdV-BDNF injected rats (1 week after injection). Note the distribution of BDNF-positive neurons throughout the cervical spinal cord, mainly in the anterior horn motoneurons in the mid to upper gray matter (**A**). High-power photomicrographs of the box area: C2 area (**B**), C3 area (**C**), C4 area (**D**), C5 area (**E**). C6 area (**F**). Injured level (at C4 segmental level: asterisk). Original magnification, ×10 (A), ×200 (B–F). Scale bar = 500 μm (A), 100 μm (B–F).

lowed sequentially by anti-rabbit IgG antibody and avidin-biotinylated peroxidase complex (Cytomation Envision + System-HRP Labeled Polymer; DAKO, Carpenteria, CA) for 3 h. After three washes in PBS, the membrane was sunk in the ECL for 1 min to take an x-ray film for visualization of peroxidase activity.

Evaluation of Cervical Motoneuron Survival

To assess the extent of spinal cord injury, the numbers of anterior horn neurons positive for Nissl, ChAT, and AChE staining were counted in each section from C1 to C8 spinal cord segments. Serial 50-μm-thick transverse sections were divided into three groups by collecting every third section separately for Nissl staining, ChAT immunostaining, and AChE immunoenzymatic staining. For Nissl staining, sections were mounted on glass slides and stained with cresyl violet. Under a microscope, large multipolar cell bodies with abundant cytoplasm and lacking the central chromatolysis in the medial, ventrolateral, and dorsolateral cell pools of the anterior horn were counted as viable motoneurons. Identification of viable motoneurons by Nissl staining and cell counting were performed as described previously (Baba et al., 1996). Using an anti-ChAT (rabbit anti-ChAT polyclonal antibody, no. AB143, 1:500; Chemicon International) as a first antibody, ChAT immunohistochemistry was performed under the same procedure following BDNF immunohistochemistry. ChAT-positive motoneurons were counted in the same manner as Nissl-positive neuron counting. Immunoenzymatic activity of AChE in the motoneurons was examined according to the method described by Hedreen et al. (1985). AChE-positive motoneurons were counted in a manner similar to that employed for Nissl-stained motoneuron cell counting.

Statistical Analysis

All measured values were expressed as mean ± standard deviation. One-way factorial analysis of variance (ANOVA) was used to compare the counted positive numbers of anterior horn motoneurons. A p value of <0.05 was considered to represent a statistically significant difference with Tukey's post hoc analysis.

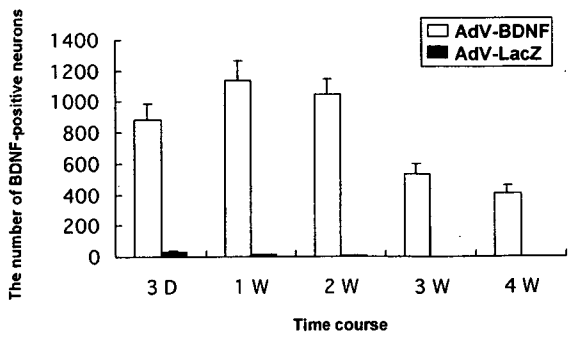

FIG. 3. Time course of BDNF-positive neurons from C1 to C8 spinal cord segments. In the AdV-LacZ injected rats, BDNF-positive neurons were nearly absent throughout the time course following injury. The number of BDNF-positive neurons reached a peak level at 1–2 weeks after injection, and the activity then decreased over the subsequent 2 weeks in the AdV-BDNF injected rats.

RESULTS

Immunohistology of BDNF Expression and Immunoblot Analysis

In AdV-BDNF injected rats, BDNF gene expression was observed mainly in the anterior horn motoneurons from 3 days to 4 weeks after spinal cord injury (Fig. 1A-A′, B-B′). In the AdV-LacZ injected rats, BDNF-positive neurons were nearly absent throughout the time course following injury (Fig. 1C-C′, D-D′). In the sagittal sections of AdV-BDNF injected rats, BDNF-positive neurons were distributed throughout the cervical spinal cord (except for injured level), mainly in the anterior horn motoneurons in the mid to upper gray matter (Fig. 2). The number of BDNF-positive neurons in AdV-BDNF injected rats reached a peak level at 1–2 weeks after injection, and the activity then decreased over the subsequent 2 weeks (Fig. 3).

Immunoblot analysis of BDNF immunoreactivity showed major molecular bands of 15 and 30 kDa. In AdV-BDNF injected rats (Fig. 4A), the bands were present from 3 days to 4 weeks after spinal cord injury, the highest peak was noted at 1–2 weeks. In AdV-LacZ injected rats (Fig. 4B), only a low-density band was observed at 3 days after spinal cord injury.

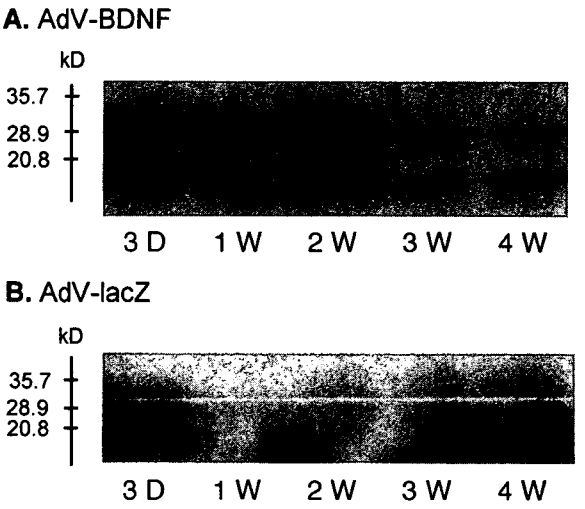

FIG. 4. Expression of BDNF evaluated by immunoblot analysis in rats injected with AdV-BDNF (**A**) or AdV-LacZ (**B**) at 3 days, 1 week, 2 weeks, 3 weeks, and 4 weeks afte spinal cord injury. In AdV-LacZ injected rats, only a low-density band was observed at 3 days after spinal cord injury. In AdV-BDNF injected rats, the band was present from 3 days to 4 weeks after the spinal cord injury and its density was significantly higher than that in AdV-LacZ-gene-injected rats.

Effects of BDNF on Nissl Staining, ChAT Immunoreactivity, and AChE Immunoenzymatic Activity

Figure 5 shows the serial changes in the numbers of surviving motoneurons, as assessed by Nissl, ChAT, and AChE staining. The number of surviving motoneurons determined by Nissl staining in AdV-BDNF injected rats from 2 weeks after spinal cord injury was significantly different from that of AdV-LacZ injected rats. The trophic effect of BDNF was also confirmed by comparing the numbers of ChAT-positive and AChE-positive cells of AdV-BDNF and AdV-LacZ injected rats. Reductions in ChAT and AChE activity were suppressed in AdV-BDNF injected rats from 2 weeks after spinal cord injury compared to those findings in AdV-LacZ injected rats. Table 2 shows the effect of BDNF on spinal cord motoneurons 2 weeks after spinal cord injury. Relative to the uninjured rats, 67 ± 8% of Nissl-stained neurons, 69 ± 9% of ChAT-stained neurons, and 64 ± 8% of

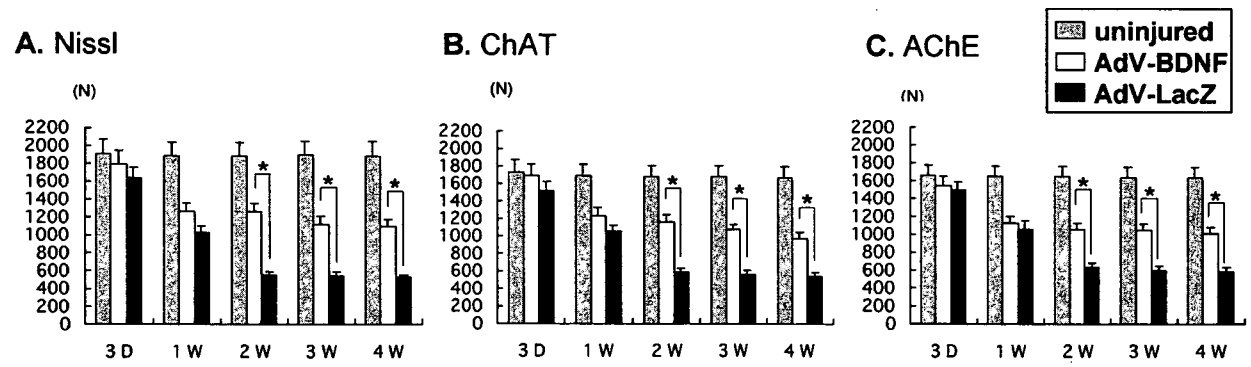

FIG. 5. Serial changes in the number of anterior horn neurons from C1 to C8 spinal cord segments with Nissl staining (**A**), ChAT immunoreactivity (**B**), and AChE activity (**C**). The number sof Nissl-positive, ChAT-positive, and AChE-positive cells was higher in AdV-BDNF injected rats from 2 weeks after spinal cord injury compared with AdV-LacZ injected rats. $*p < 0.05$, compared with AdV-BDNF injected rats. A statistically significant difference compared with uninjured rats was excluded in this graph. Data are mean ± SD of 10 rats in each group.